Check for updates

Facile synthesis and microwave absorption investigation of activated carbon@Fe_3O_4 composites in the low frequency band

Pengfei Yin, [ID][a] Yu Deng,*[b] Limin Zhang,[c] Ning Li,[c] Xing Feng,[a] Jian Wang[a] and Yi Zhang[a]

Activated carbon@Fe_3O_4 composites with good electromagnetic wave absorption performances in the low frequency range were synthesized *via* the hydrothermal method. The crystal structure, microstructure, magnetization properties, frequency-dependent electromagnetic properties and microwave absorption properties of the as-prepared composites were characterized *via* XRD, VSM, SEM, TEM and VNA, respectively. The results indicated that the electromagnetic wave absorption performance of the composites can be adjusted through the addition of activated carbon. A suitable loading content of Fe_3O_4 NPs on activated carbon can also enhance the microwave absorption performance of the composites. The synergy of dielectric and magnetic loss is the main electromagnetic wave absorption mechanism, and the maximum RL of −10.08 dB at 1.75 GHz with a −5 dB bandwidth over the frequency range of 1.55 GHz (1.07–2.62 GHz) is obtained when the percentage of Fe_3O_4 NPs and the thickness of the composites are 74 wt% and 5 mm, respectively. Hence, the composite reported in this study can be used as a promising microwave absorbing material in the low frequency range of 0.5–3 GHz.

1. Introduction

Nowadays, with the rapid development of modern radars and electronic devices, increasing attention has been given to electromagnetic wave absorbing materials within the GHz range.[1–4] However, in particular, the detection frequency band of ship-based phased array radars used today is located in the low frequency range of the S-band, and the working frequency range of many space-based radars has been extended to 1.2 GHz thus far. In addition, the radiant frequency range of electronic devices used in daily life is focused in the low frequency band. Nevertheless, the existing investigations on electromagnetic wave absorbing materials are mainly focused on the 2–18 GHz range, and the microwave absorption of these materials is very poor in the low frequency electromagnetic wave region, particularly in the range of 1–2 GHz. This poses a significant challenge in the design and development of materials with good absorption ability in the low frequency band.[5,6]

In recent years, a variety of materials that can attenuate electromagnetic waves by dissipating them *via* interference or converting them into heat have been studied extensively, including dielectric materials,[7,8] magnetic metals,[9,10] conductive macromolecules,[11,12] and ferrites. Among them, carbon materials have been extensively investigated due to their excellent properties, such as outstanding chemical stability, high electrical conductivity, and unique structures.[13–15] However, it is almost impossible obtain excellent electromagnetic wave absorption performance using unmodified carbon materials due to unilateral dielectric loss. Thus, to optimize the properties of carbon materials as electromagnetic wave absorbers, they need to be modified and composited with other nanomaterials possessing different electromagnetic loss mechanisms, which is a promising way to improve their microwave absorption properties.[16,17]

During the past decades, numerous investigations have been conducted to decorate carbon materials with ferrites to prepare magnetic nanoparticles due to their special magnetic properties, strong absorption performance, low cost, *etc.* Heidari *et al.*[18] researched the microwave absorption performance of $ZnO/Fe_3O_4/GO$ nanocomposites in the frequency range of 5–8 GHz. Their results showed that the dispersion of nanoparticles can be improved by increasing the homogenizer speed, which leads to an increase in absorption bandwidth; also, graphene oxide has an important effect on absorption compared with the composites without graphene oxide. Wang *et al.*[19] fabricated hollow $ZnFe_2O_4$ microspheres@rGO decorated with TiO_2 nanosheets *via* a two-step hydrothermal method. The electromagnetic wave absorption properties of the $ZnFe_2O_4$@rGO@TiO_2 composites indicate that their maximum reflection loss can be enhanced significantly, achieving −55.6 dB at 3.8

[a]*College of Science, Sichuan Agricultural University, Ya'an 625014, P. R. China*

[b]*College of Water Conservancy and Hydropower Engineering, Sichuan Agricultural University, Ya'an 625014, P. R. China. E-mail: yudeng21@sicau.edu.cn*

[c]*Key Laboratory of Space Applied Physics and Chemistry (Ministry of Education), School of Science, Northwestern Polytechnical University, Xi'an 710072, P. R. China*

GHz for a coating thickness of 2.5 mm, and the maximum absorption bandwidth exceeding −10 dB was about 6.4 GHz. Hou et al.[20] fabricated $MWCNTs/Fe_3O_4$ composites via the hydrothermal synthesis method, and their microwave absorption performance was also studied in the frequency range of the X-band. With an increase in the content of Fe_3O_4, the maximum reflection loss of −18.22 dB at 12.05 GHz was achieved for enhancing the magnetic loss of the composites. Sardarian et al.[21] prepared $Fe_3O_4/BaTiO_3@MWCNT$ ternary composites and investigated the synergistic mechanism of their enhanced microwave absorption performance; the microwave absorption of the composites improved in the low frequency band with an increase in the content of magnetic particles.

Among the present investigations, various types of carbon materials have been widely studied, such as CNTs (MWCNTs), graphene (graphene oxide), and carbon fibers, while the microwave absorption performance of activated carbon has rarely been reported. Activated carbon is also a type of favourable carrier in many areas due to its loose structure. Moreover, as a type of magnetic ferrite, Fe_3O_4 has been extensively used to absorb electromagnetic waves due to its high magnetic loss and Curie temperature.[22] However, the imaginary part of the permeability is much larger than that of the permittivity in pure Fe_3O_4 particles, which leads relatively poor impedance matching. Thus, combining Fe_3O_4 particles with activated carbon may be a promising route to improve their electromagnetic wave absorption performance.

Therefore, due to its excellent dielectric properties, activated carbon was employed as a dielectric absorbent carrier to composite with Fe_3O_4 nanoparticles (denoted as Fe_3O_4 NPs henceforth) in this study. The as-prepared activated carbon@Fe_3O_4 composites were synthesized via the hydrothermal method due to its high efficiency and convenience. In addition, the phase identification, microstructure, magnetization curves and microwave absorption properties of the as-prepared composites were characterized via XRD, VSM, SEM, TEM and Vector Network Analysis (VNA), respectively. The results indicated that the activated carbon@Fe_3O_4 composites can be used as a new candidate for microwave absorption in the low frequency band of 0.5–3 GHz.

2. Experimental

2.1. Synthesis of activated carbon@Fe_3O_4 composites

Analytically pure activated carbon micropowder, used in our investigation, was purchased from Chongqing MaoYe Chemical Reagent Co. Ltd, China. Fe_3O_4 NPs coated on activated carbon were prepared via the hydrothermal synthesis method.[23] In detail, 3.95 g ferric chloride hexahydrate ($FeCl_3 \cdot 6H_2O$) was added to 80 mL ethylene glycol to form a clear solution. Then, 8.75 g sodium acetate trihydrate (NaAc) and different amounts of activated carbon were consecutively added into the above-mentioned solution with continuous stirring and ultrasonic dispersion for 30 min. Subsequently, the obtained mixed solution was directly sealed into a 100 mL Teflon-lined stainless-steel autoclave and the temperature was maintained at 200 °C for 12 h. After cooling the autoclave to room temperature, the

precipitate was separated from the solution using a magnet. Then, the as-prepared black product was washed with distilled water and ethanol three times, in sequence, and dried at 50 °C for 6 h. To understand the influence of the Fe_3O_4 NPs content on the microwave absorption performance, five samples containing 0, 27, 53, 74, and 100 wt% Fe_3O_4 NPs (denoted as activated carbon, 27% Fe_3O_4, 53% Fe_3O_4, 74% Fe_3O_4 and pure Fe_3O_4, respectively) were prepared using the same method described above. Ferric chloride hexahydrate and NaAc were purchased from Chengdu KeLong Chemical Reagent Co. Ltd, China, and ethylene glycol was purchased from Sinopharm Chemical Reagent Co. Ltd, China. All chemicals were analytical pure and used without further purification.

2.2. Characterization

The microstructure and elemental distribution of the composites were observed and investigated via scanning electron microscopy (SEM) on a Hitachi S-4800 and transmission electron microscopy (TEM) on a JTM-2100. The crystal structure and phase components were measured by the Rigaku D/MAX-2004 X-ray diffractometer with Cu-K$_\alpha$ radiation ($\lambda = 0.15418$ nm). The magnetization curves of the composites were determined on a Q-VSM vibrating specimen magnetometer (VSM). Paraffin was employed as the agglomerant to adhere the activated carbon@Fe_3O_4 particles, and a physical hybrid method was used to prepare the activated carbon@Fe_3O_4/paraffin composites with the mass ratio of activated carbon@Fe_3O_4 and paraffin fixed at 1 : 1 because the mixtures would have become very hard to shape when the particles were overloaded. Then, the produced mixtures were pressed into a toroidal shape with an outer diameter of 7 mm, inner diameter of 3.04 mm, and thicknesses of 2–5 mm. Thus, the S-parameters (i.e. S_{11} and S_{21}) could be measured with the coaxial transmission and reflection method at 0.5–3 GHz on a TIANDA TD3618C Vector Network Analyzer, and the details of the practical measurement process at room temperature are shown in Fig. 1. Finally, the electromagnetic parameters (i.e. relative complex permittivity and permeability) of the composites were calculated according to the theory of Nicolson and Ross.[24]

The dielectric loss tangent, magnetic loss tangent and frequency dependent Z_{in}/Z_0 values of the activated carbon@Fe_3O_4/paraffin composites were calculated based on the transmission line theory and the electromagnetic
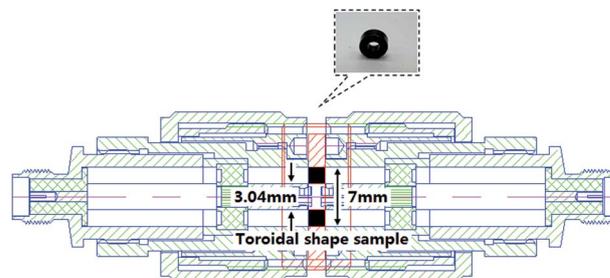

Fig. 1 Measurement of S-parameters using the coaxial transmission and reflection method.

parameters measured above. The input impedance Z_{in} can be expressed as follows:[25]

$$Z_{in} = Z_0 \sqrt{\frac{\mu_r}{\varepsilon_r}} \tanh\left(j \frac{2\pi fd}{c} \sqrt{\mu_r \varepsilon_r}\right) \quad (1)$$

where d is the thickness of the material, f the frequency, c the velocity of light, μ_r the relative complex permeability, and ε_r the relative complex permittivity. Therefore, the reflection loss (henceforth denoted as RL) of incident electromagnetic waves at the surface of the absorbing materials is given as follows:

$$RL = 20 \log \left| \frac{Z_{in} - Z_0}{Z_{in} + Z_0} \right| \quad (2)$$

where Z_0 is the impedance of air. In addition, the entire computation procedure was programmed with Matlab language, which was used to calculate the electromagnetic parameters, dielectric and magnetic loss tangent, and the final microwave reflection loss.

3. Results and discussion

The crystal structures of the activated carbon@Fe$_3$O$_4$ composites were measured using an XRD diffractometer. Fig. 2 presents the diffraction patterns of the as-prepared samples. The characteristic diffraction peaks at $2\theta = 31.24°$, $36.82°$, $44.76°$, $55.62°$, $59.30°$ and $65.19°$ are in good agreement with the (220), (311), (400), (422), (511) and (440) planes of Fe$_3$O$_4$, respectively, as reported in the standard card (JCPDS card no. 26-1136).[26] Also, the peak at about $2\theta = 26.20°$ is assigned to the (002) plane of the fluffy structured activated carbon (JCPDS card no. 26-1076).[27] It is observed that the intensity of the Fe$_3$O$_4$ diffraction peaks enhance with an increase in the Fe$_3$O$_4$ NP loading content and that of the activated carbon decrease during the same process. This above phenomenon suggests that the Fe$_3$O$_4$ NPs may be successfully introduced on the fluffy structured activated carbon.
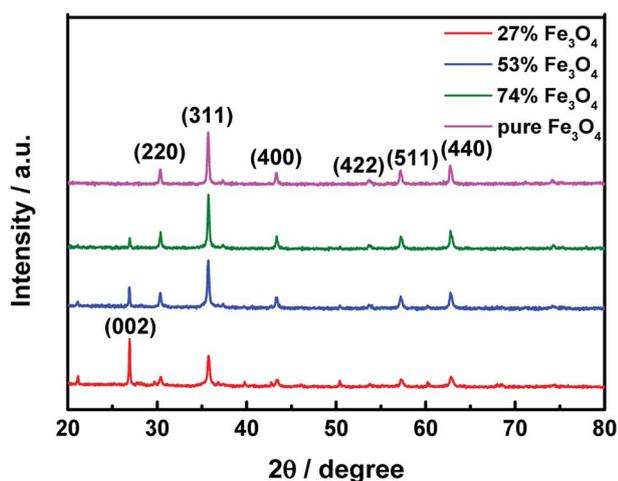

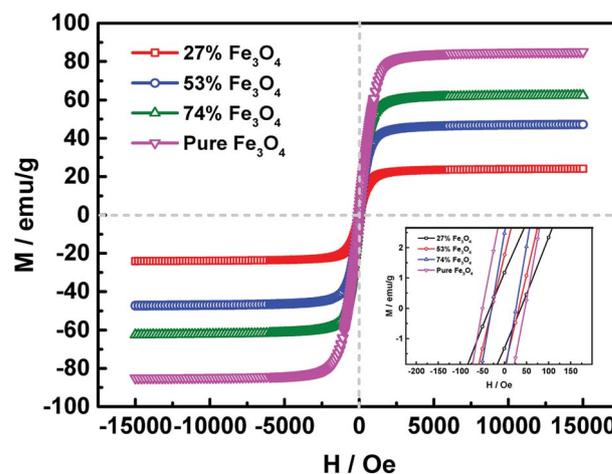Fig. 2 X-ray diffraction patterns of the activated carbon@Fe$_3$O$_4$ absorbing composites.

Fig. 3 Hysteresis loops of the activated carbon@Fe$_3$O$_4$ composites and pure Fe$_3$O$_4$ NPs.

To verify the magnetic properties of the as-prepared samples, their hysteresis loops were measured using VSM at room temperature, as shown in Fig. 3. It is observed that the saturation magnetization of the composite is strongly related to the loading content of Fe$_3$O$_4$ NPs, and higher loading content leads to larger saturation magnetization. The saturation magnetization values of 24.07 emu g^{-1}, 47.25 emu g^{-1}, 62.43 emu g^{-1} and 85.05 emu g^{-1} correspond to 27% Fe$_3$O$_4$, 53% Fe$_3$O$_4$, 74% Fe$_3$O$_4$ and pure Fe$_3$O$_4$ NPs, respectively. Moreover, the remanences and coercivities of the samples are both relatively low, which suggests that the hysteresis loops of the composites exhibit typical paramagnetic behavior.

Fig. 4 shows the microstructures of activated carbon, Fe$_3$O$_4$ NPs and activated carbon@Fe$_3$O$_4$ composites. It shows that the size of the activated carbon is much larger than that of the Fe$_3$O$_4$ NPs prepared via the hydrothermal synthesis method, and the surface of the activated carbon is relatively irregular. The fine Fe$_3$O$_4$ NPs present a ball-like structure and many of them form porous structures by agglomerating with each other. When the loading of the Fe$_3$O$_4$ NPs was relatively low in the composites, there were only a few Fe$_3$O$_4$ NPs loaded on the surface of the activated carbon in the field of view, as shown in Fig. 4(b). This is because the density of activated carbon is much lower than that of Fe$_3$O$_4$. Thus, a low mass content of Fe$_3$O$_4$ results in the amount of activated carbon particles being much more than that of the Fe$_3$O$_4$ NPs. Therefore, the loading capacity of Fe$_3$O$_4$ NPs on the activated carbon is relatively low. This situation was improved when the mass content of Fe$_3$O$_4$ was 53 wt%, where the activated carbon particles were dispersed in the agglomerations of Fe$_3$O$_4$ NPs. However, it was observed that some of the activated carbon particles were not coated well by the agglomerated Fe$_3$O$_4$ NPs, as shown in Fig. 4(c). Nevertheless, as shown in Fig. 4(d), the loading capacity was significantly enhanced with a further increase in the content of Fe$_3$O$_4$ NPs, and most of the activated carbon particles were coated by the agglomerated Fe$_3$O$_4$ NPs. To the best of our knowledge, activated carbon is a dielectric loss absorber, and the microwave
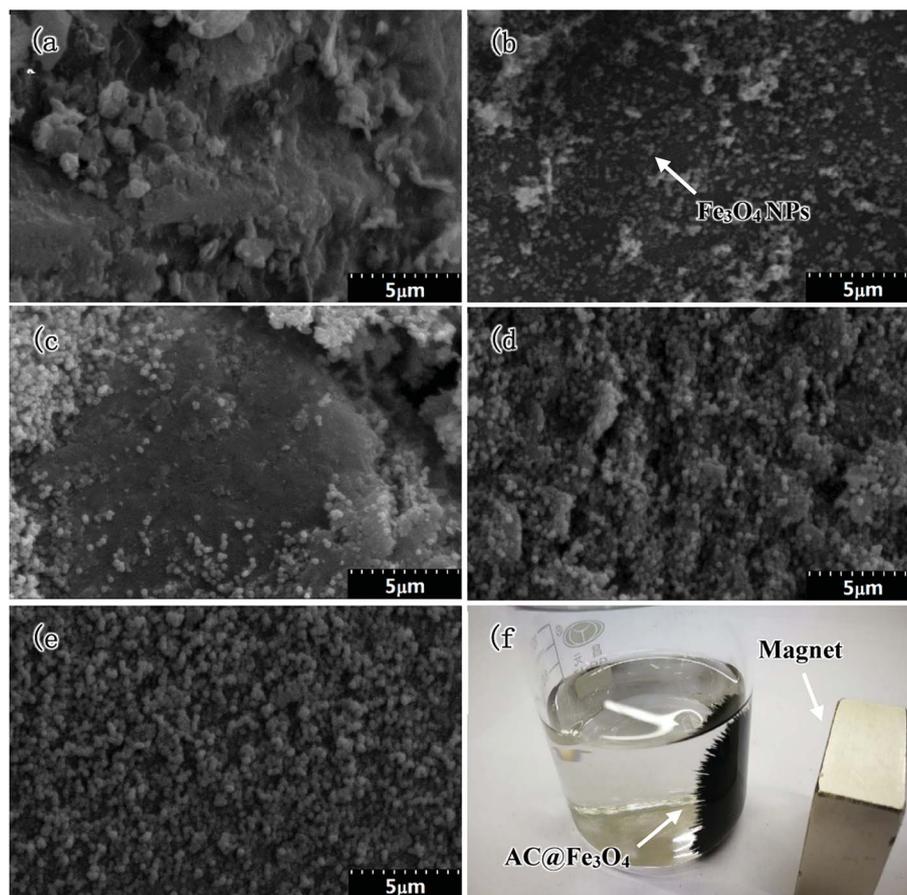
Fig. 4 SEM images of activated carbon (a), 27 wt% Fe_3O_4 (b), 53 wt% Fe_3O_4 (c), 74 wt% Fe_3O_4 (d) and pure Fe_3O_4, (e) and macro-morphology of the activated carbon@Fe_3O_4 composite (f).

absorption of Fe_3O_4 NPs mainly depends on magnetic loss. It is common knowledge that a modest ratio of complex permeability and permittivity is an important factor in determining the impedance matching of absorbing materials. Thus, the improved impedance matching of the activated carbon@Fe_3O_4 composites plays an important role in increasing their microwave absorption. Furthermore, the as-prepared composites are paramagnetic and can be attracted by a magnet due to the loading of Fe_3O_4 NPs on activated carbon, which is shown in Fig. 4(f).

The TEM images and corresponding elemental distributions of the composite with 74 wt% Fe_3O_4 NPs are shown in Fig. 5. As shown in Fig. 5(a), the as-prepared Fe_3O_4 NPs are all close to spherical in shape with particle sizes mainly concentrated at about 250 nm. From the HR-TEM image in Fig. 5(b), the good grain orientation of a single Fe_3O_4 nanoparticle can be observed clearly, and the SAED pattern in this region also demonstrates the crystalline feature of the Fe_3O_4 NPs. Furthermore, the crystal lattice fringes with a spacing of 0.256 nm can be assigned to the (311) plane of Fe_3O_4, which is in accordance with the XRD results. In addition, the distribution of elements in the activated carbon@Fe_3O_4 composite was determined from the corresponding elemental mapping images, as shown in Fig. 5(c–f), in which it can be observed clearly that the composite consists of

Fe, O and C elements. The distribution area of C is significantly larger than the corresponding areas of Fe and O, indicating that the Fe_3O_4 NPs are distributed on the surface of the activated carbon. Thus, combined with the XRD, VSM and SEM results, we can conclude that the Fe_3O_4 NPs adhered tightly to the surface of the activated carbon.

Furthermore, electromagnetic wave absorption performance of the activated carbon@Fe_3O_4 composites was investigated. Fig. 6 displays the complex permittivity ($\varepsilon = \varepsilon' - j\varepsilon''$) and permeability ($\mu = \mu' - j\mu''$) of activated carbon@$Fe_3O_4$ composites, which were calculated from the S-parameters measured earlier. These electromagnetic parameters are very important in determining the dielectric and magnetic loss of microwave absorption composites, and the transmission and reflection of electromagnetic waves during the absorption process are also affected by them.[28] From Fig. 6(a) and (b), it can be observed that the real part of permittivity of all the samples decrease with an increase in frequency, and the content of Fe_3O_4 NPs has a significant effect on the real part of permittivity of the as-prepared composite, which increases with an increase in the Fe_3O_4 NPs loading on the activated carbon. In contrast, the values of the imaginary part first increased and then decreased as the frequency increased. It can be noted that the imaginary part of the pure Fe_3O_4 NPs is larger when the
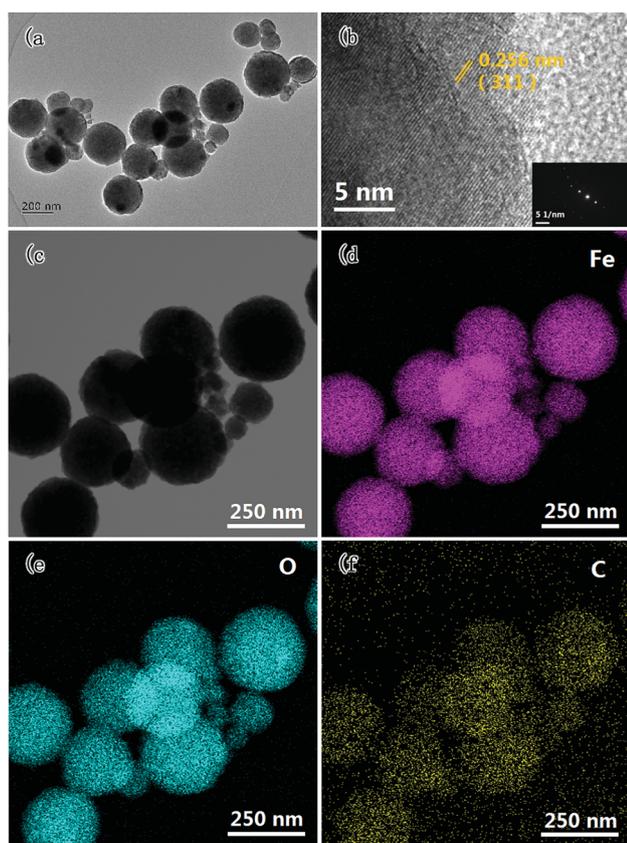
Fig. 5 TEM image (a), HR-TEM image (b), and corresponding elemental mapping images (c–f) of the activated carbon@Fe_3O_4 composites.

frequency is relatively lower, and it decreases rapidly as the frequency increases. However, this situation can be improved with the addition of activated carbon, although the values of the imaginary part of the composites decrease to some extent in the low-frequency domain. The imaginary part of the composite with 74 wt% Fe_3O_4 NPs shows a relatively higher value throughout the measurement range among the samples. Usually, the imaginary part of permittivity represents the dielectric dissipation ability of microwave energy,[29] which indicates that the dissipation ability of the composite with 74 wt% Fe_3O_4 NPs may be better in the entire frequency range. Moreover, we can find that the complex permittivity of the composites exhibits evident frequency dependent dielectric properties. Generally, in the gigahertz frequency range, the permittivity presents a strong dependence on inherent dipole polarization and interfacial polarization, and the displacement current generated from this process always lags behind the build-up potential when the frequency increases. Thus, the real and imaginary parts of permittivity present frequency-related properties.[30] Moreover, it is clear that there is a slight effect on the enhancement of the imaginary part of permittivity when the content of Fe_3O_4 NPs is lower. Hence, it can be concluded that fewer Fe_3O_4 NPs loaded on activated carbon may have not much effect on enhancing the polarization. Besides, according to the relationship between resistivity and the imaginary part of permittivity:[31]

$$\rho = \frac{1}{\omega \varepsilon_0 \varepsilon''} \quad (3)$$

where, ρ is the resistivity, ε_0 the dielectric constant of free space, and ω the angular frequency. Therefore, the resistivity of the composite with 74 wt% Fe_3O_4 NPs is the maximum at 3 GHz and minimum at 0.5 GHz among the as-prepared samples, and the resistivity of the composites can be adjusted under the measured frequency range by controlling the content of Fe_3O_4 NPs loaded on activated carbon.

Fig. 6(c) and (d) display the real and imaginary parts of permeability as a function of frequency. It is observed that the real part of permeability only slightly increases when the loading content of Fe_3O_4 NPs is low. However, it is significantly enhanced with a further increase in Fe_3O_4 NPs. This is because the real part of permeability is related to saturation magnetization, M_s, as follows:[32]

$$\mu' \propto 4\pi M_s \quad (4)$$

Also, the M_s of the composites increases significantly with higher loading of Fe_3O_4 NPs, which leads to the enlargement of the real part of permeability. Besides, it is evident that the real part of permeability of the composites with different loading contents of Fe_3O_4 NPs increases with an increase in frequency. Moreover, the imaginary part of permeability of the composites has the same variation trend as the real part of permeability; the difference is that a smooth peak value of 2.92 at 2.83 GHz could be observed when the loading content of Fe_3O_4 NPs is 74 wt%. This demonstrates that the excessive loading of Fe_3O_4 NPs is unable to enhance the imaginary part of permeability further in the high frequency domain. It is due to that the resonance peak in the imaginary part is ascribed to the domain wall resonance and natural resonance of Fe_3O_4 NPs loaded on the activated carbon.[33]

In addition, it can be noted that the complex permittivity and permeability of the activated carbon@Fe_3O_4 composites are significantly lower than that of the Fe_3O_4 NPs. The permittivity and permeability of the composites can be adjusted with the addition of activated carbon because the complex permittivity and permeability of activated carbon are much less than that of the Fe_3O_4 NPs. Hence, the permittivity and permeability of the activated carbon@Fe_3O_4 composites are reduced with the addition of activated carbon, which indicates that the μ'/ε' ratio of the activated carbon@Fe_3O_4 composites can be adjusted in different frequency domains by controlling the content of activated carbon. According to the impedance matching theory, the incident microwaves can have much easier access to the materials to be dissipated when their permeability is closer to their permittivity, which is beneficial to improve the microwave absorption properties of the composites.

Fig. 7(a) and (b) show the dielectric and magnetic loss tangent as a function of frequency, which can be calculated based on the measured electromagnetic parameters above. The results indicate that the dielectric loss tangent of the pure Fe_3O_4 NPs first increases and then decreases as the frequency increases, particularly in the high frequency domain, it
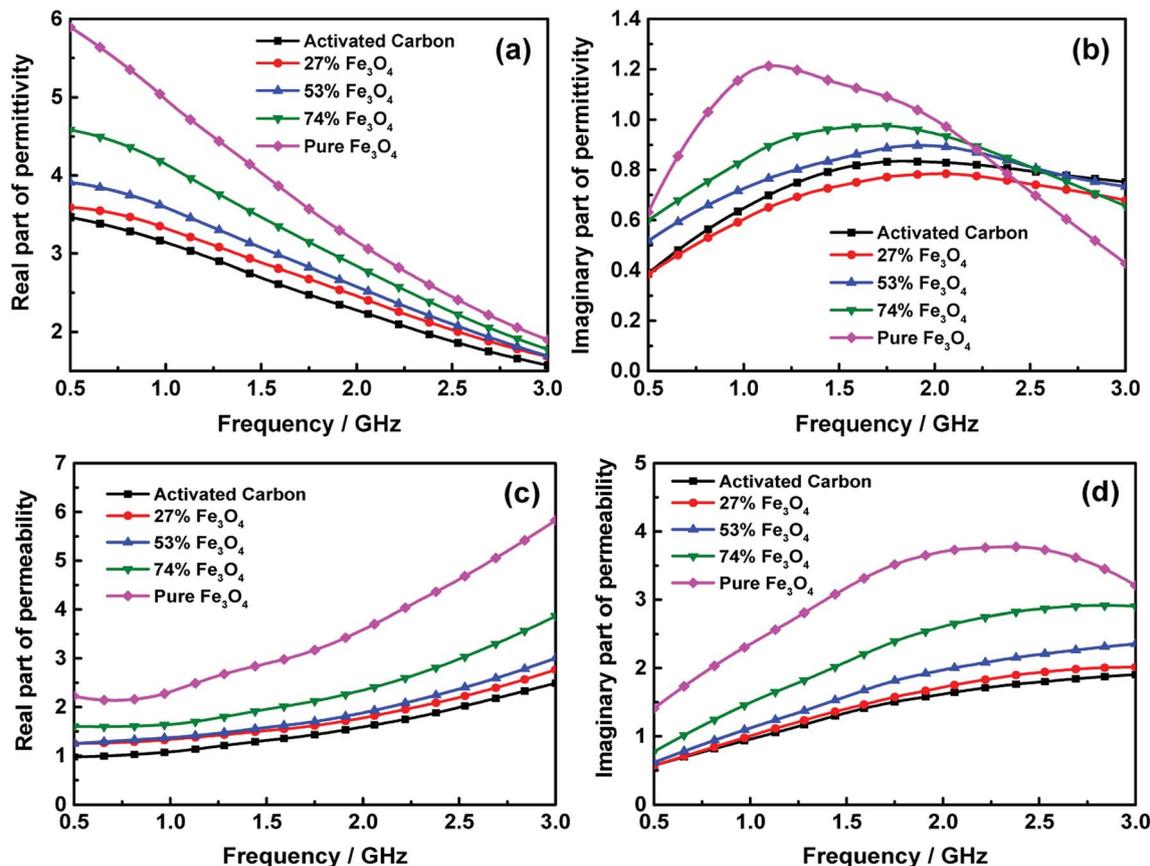
Fig. 6 Frequency dependence of the real part (a) and imaginary part (b) of complex permittivity, and real part (c) and imaginary part (d) of complex permeability of the activated carbon@Fe$_3$O$_4$ composites with thickness of 5 mm.

decreases rapidly. In contrast, the dielectric loss tangent of the activated carbon increases continuously with an increase in frequency, which demonstrates the excellent dielectric loss properties of activated carbon. Consequently, the loading of Fe$_3$O$_4$ NPs on activated carbon takes advantage of this superiority to improve the dielectric loss properties of the pure Fe$_3$O$_4$ NPs in the high frequency domain. Moreover, it can be noted that the magnetic loss tangent of the Fe$_3$O$_4$ NPs is a slightly

larger than that of the activated carbon in the low frequency domain; nonetheless, it reduces sharply as the frequency increases. The magnetic loss tangent of the composite with 74 wt% Fe$_3$O$_4$ NPs is relatively higher in the entire measured frequency range with a peak value of 1.13 at 1.8 GHz. This is mainly because the morphology of the Fe$_3$O$_4$ NPs prepared *via* the hydrothermal synthesis method is ball-like. In fact, the flake-shaped particles with planar anisotropy have higher
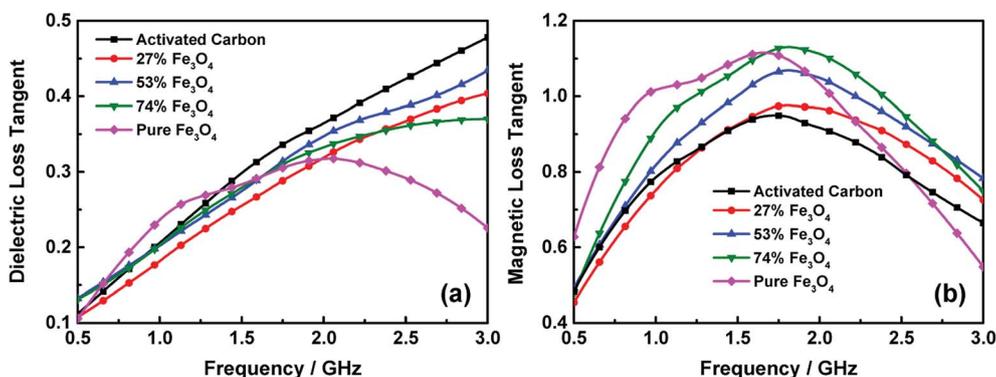

Fig. 7 Frequency dependence of the dielectric loss tangent (a) and magnetic loss tangent (b) of the activated carbon@Fe$_3$O$_4$ composites with thickness of 5 mm.

magnetic loss tangent than the sphere-shaped particles due to their higher Snoek's limits,[34–36] which leads to the magnetic loss properties of the as-prepared pure Fe_3O_4 NPs not being sufficiently large. Nevertheless, the loading of the Fe_3O_4 NPs on activated carbon may modify the magnetic loss properties of the composites to a certain extent, and the magnetic loss tangent slightly increases with an increase in the Fe_3O_4 NPs loading content.

Furthermore, it can be noted that the dielectric and magnetic loss tangent of the composites can both achieve higher values when the loading content of Fe_3O_4 NPs on activated carbon is within a proper range. This is because the interface polarization is enhanced with an increase in charges transferring through the interfaces between the Fe_3O_4 NPs and activated carbon. Moreover, it can be also found that the magnetic loss tangent is only slightly larger than the dielectric loss tangent, which indicates that both the dielectric and magnetic loss contribute to the microwave absorption in the as-prepared composites.

Usually, the microwave reflection loss can be used to characterize the microwave absorption properties of materials. Fig. 8 presents the microwave reflection losses of the activated carbon@Fe_3O_4 composites with different absorption thicknesses, which were calculated according to the measured electromagnetic parameters and transmission line theory. As shown in Fig. 8(a), the reflection loss of the electromagnetic wave increases as the frequency increases. Moreover, the RL curve is enhanced with an increase in the loading content of Fe_3O_4 NPs. Also, no electromagnetic wave absorption peak was

observed in the measurement range when the thickness of the composites was 2 mm. In addition, compared to the pure Fe_3O_4 NPs, it is interesting to note that the electromagnetic wave absorption ability of the composite is stronger when the loading content of Fe_3O_4 NPs is 74 wt%, which indicates that the microwave absorption properties are enhanced when a suitable content of activated carbon was added. This is because the electromagnetic wave absorption of the pure Fe_3O_4 NPs is mainly due to natural resonance and domain wall resonance, and the addition of activated carbon in a suitable range could introduce the dielectric loss of activated carbon and also enhance the interface polarization between the interface of the Fe_3O_4 NPs and activated carbon. The absorption bandwidths with an RL curve lower than −5 dB at the thickness of 2 mm are 0 GHz, 0 GHz, 0.11 GHz (2.89–3 GHz), 0.74 GHz (2.26–3 GHz) and 0.53 GHz (2.47–3 GHz), which correspond to the activated carbon, 27% Fe_3O_4, 53% Fe_3O_4, 74% Fe_3O_4 and pure Fe_3O_4, respectively. Nevertheless, the bandwidths of the composites add up to 0.34 GHz (2.66–3 GHz), 0.48 GHz (2.52–3 GHz), 0.44 GHz (2.56–3 GHz), 1.34 GHz (1.66–3 GHz) and 1.1 GHz (1.9–3 GHz) when the thickness of the sample is 3 mm. Also, in particular, a single absorption peak of 74% Fe_3O_4 starts to appear because the materials with increased thickness exhibited more efficient microwave absorption.

The microwave reflection losses of the activated carbon@Fe_3O_4 composites at the thickness of 4 mm are shown in Fig. 8(c), which demonstrates that the maximum RL peaks of the samples appeared in this measurement range. However, the absorption intensity of the 74 wt% Fe_3O_4 composite is almost
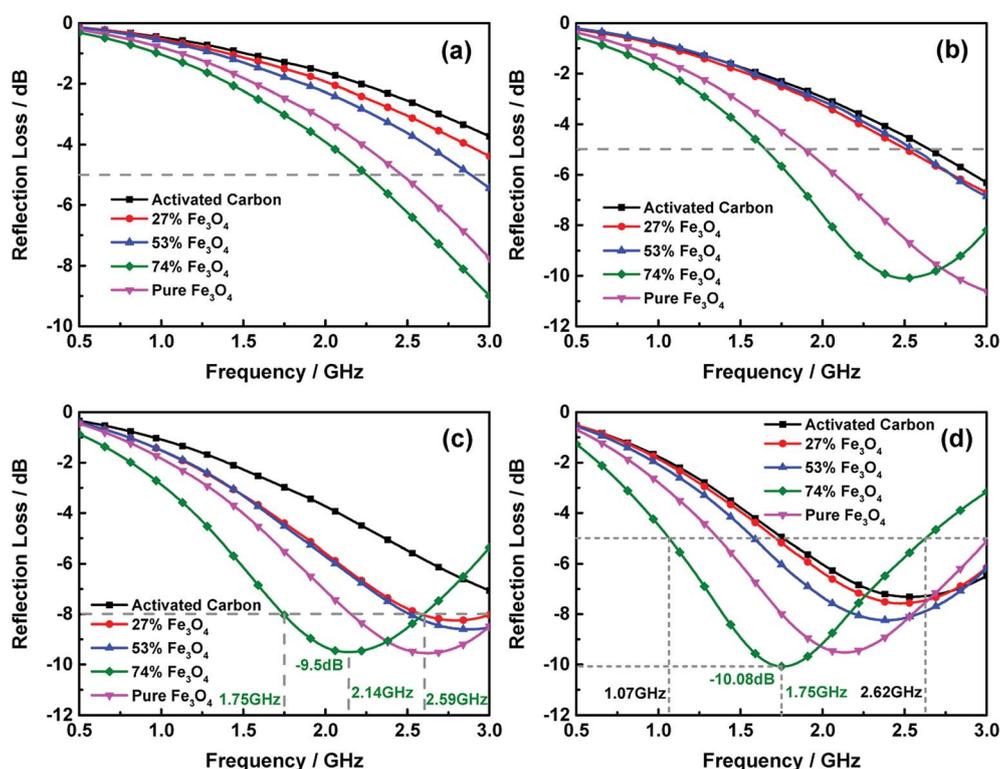

Fig. 8 Frequency dependence of the microwave reflection loss curves at different thicknesses of 2 mm (a), 3 mm (b), 4 mm (c) and 5 mm (d).
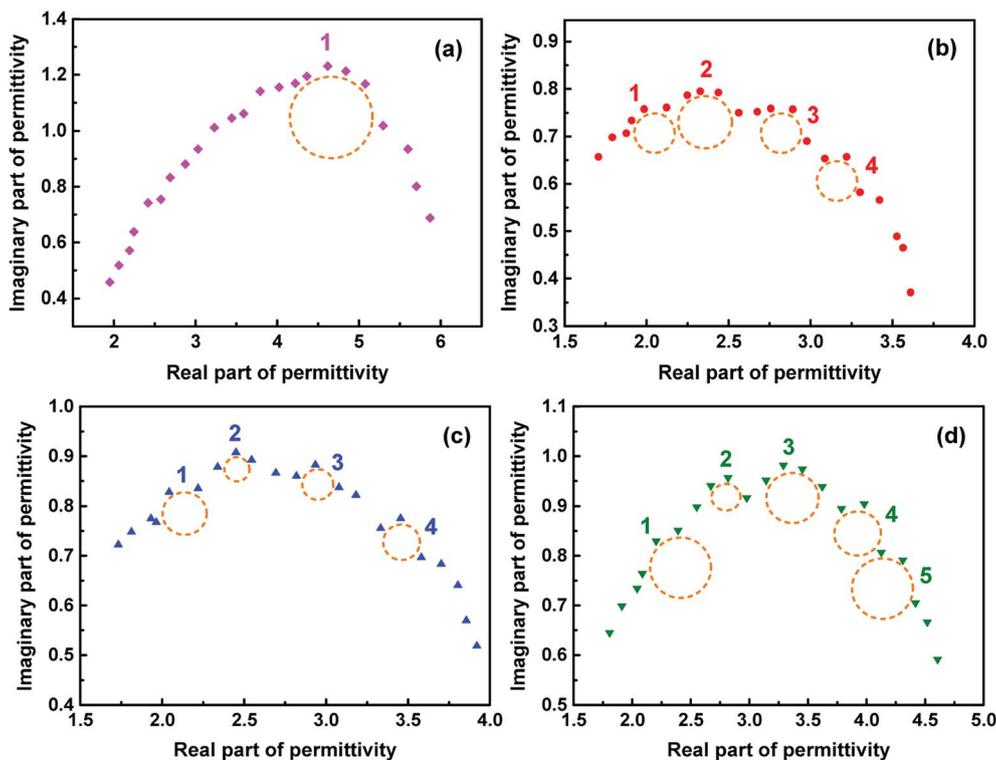
Fig. 9 Plots of $\varepsilon' - \varepsilon''$ for pure Fe_3O_4 (a), 27% Fe_3O_4 (b), 53% Fe_3O_4 (c) and 74% Fe_3O_4 (d) with thickness of 5 mm.

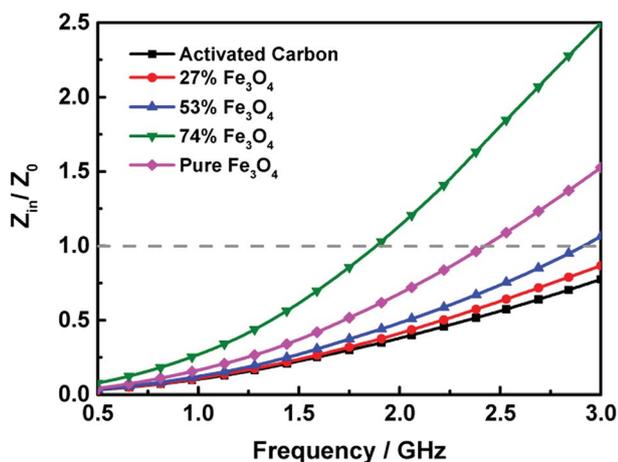**Fig. 10** Frequency dependent Z_{in}/Z_0 values of the activated carbon@Fe_3O_4 composites with thickness of 5 mm.

the same as that of pure Fe_3O_4, while both the RL peak position and bandwidth of the former are relatively lower. Thus, it is clear that the electromagnetic wave absorption performance of the Fe_3O_4 NPs in the low frequency band can be improved by loading them on activated carbon with a suitable content, *e.g.*, the maximum reflection loss is −9.5 dB at 2.14 GHz with a −8 dB bandwidth over the frequency range of 0.84 GHz (1.75–2.59 GHz) when the content of Fe_3O_4 NPs is 74 wt%.

The as-prepared activated carbon@Fe_3O_4 composites have greater effect on the microwave absorption in the measurement

frequency range when their thickness is 5 mm, and their RL curves are presented in Fig. 8(d). It can be observed that reflection absorption peaks appeared in all the samples with different loading contents of Fe_3O_4 NPs, and the position of the RL peaks also shifted to a lower frequency range, particularly for the 74 wt% Fe_3O_4 sample. This is due to the quarter wavelength resonance effect, and the matching mode can be expressed as follows:[37]

$$f = \frac{nc}{4d\sqrt{\mu_r \varepsilon_r}} \qquad (5)$$

where d is the thickness of the absorber, c the velocity of light in free space, ε_r the complex permittivity, and μ_r the complex permeability. From eqn (5), we can easily find that the resonance frequency is strongly dependent on the thickness of the absorber. Hence, both the position and peak value of the maximum RL moved to a lower frequency range as the thickness of the absorber increased. Moreover, this result also suggests that a suitable loading content of Fe_3O_4 NPs on the activated carbon can enhance the electromagnetic wave absorption performance of the composites. Furthermore, the position, intensity, and absorption bandwidth of the absorption peak can also be adjusted. The maximum RL of the 74 wt% Fe_3O_4 sample is −10.08 dB at 1.75 GHz with a −5 dB bandwidth over the extended frequency range of 1.55 GHz (1.07–2.62 GHz). This is because the primary electromagnetic wave absorption mechanisms of the Fe_3O_4 NPs are natural resonance and domain wall resonance, while the absorption of the activated carbon depends on dipole polarization, as mentioned above.

Table 1 Comparison of the microwave absorption performances between the activated carbon@Fe_3O_4 composites and other representative composites reported in the recent literature

Material	Thickness	RL < −5 dB	RL < −10 dB	Minimum RL	Ref.
AC@Fe_3O_4 (74% NPs)	2 mm	2.26–3 GHz	—	−8.99 dB	This work
AC@Fe_3O_4 (74% NPs)	3 mm	1.66–3 GHz	—	−10.09 dB	This work
AC@Fe_3O_4 (74% NPs)	4 mm	1.35–3 GHz	—	−9.51 dB	This work
AC@Fe_3O_4 (74% NPs)	5 mm	1.07–2.62 GHz	—	−10.08 dB	This work
ZnO/Fe_3O_4/GO	2 mm	6.4–8 GHz	—	−7.2 dB	18
$ZnFe_2O_4$@rGO@TiO_2	2.5 mm	—	2.8–5.4 GHz	−55.6 dB	19
MWCNTs/Fe_3O_4	2 mm	—	10.9–12.4 GHz	−18.22 dB	20
GO/CNT-Fe_3O_4	5 mm	—	3.5–4.5 GHz	−37.3 dB	41
PANI/Fe_3O_4/MWCNT	4 mm	—	8–15 GHz	−16 dB	42

Consequently, the electromagnetic wave absorption mechanism of the activated carbon@Fe_3O_4 composite will have a synergetic effect from its different components, i.e., its final electromagnetic wave absorption is a synergy of dielectric and magnetic loss.[38] Moreover, the interface polarization between the surfaces of the two components will also contribute to the absorption. This is because the real and imaginary parts of permittivity will satisfy the follow equation according to the Debye theory:[39]

$$(\varepsilon' - \varepsilon_\infty)^2 + (\varepsilon'')^2 = (\varepsilon_s - \varepsilon_\infty)^2 \tag{6}$$

where ε_∞ is the dielectric constant at infinite frequency, and ε_s the static dielectric constant. Hence, the ε'–ε'' curve deduced from eqn (6) would be in the form of a semicircle, which is termed as the Cole–Cole semicircle and is caused by one Debye dipolar relaxation of heterogeneous interface polarization. The ε'–ε'' curves of the composites with thickness of 5 mm are displayed in Fig. 9, which indicates that there is only one Cole–Cole semicircle for the Fe_3O_4 NPs, as shown in Fig. 9(a). This indicates that there is a single relaxation process for the pure Fe_3O_4 NPs. However, it can be observed that the plots of the activated carbon@Fe_3O_4 composites have more semicircles, suggesting that the addition of activated carbon results in multiple dielectric relaxation processes in the composites. This is attributed to the interface polarization generated at the interfaces between the Fe_3O_4 NPs and activated carbon. In particular, the 74 wt% Fe_3O_4 composite presents five distinct Cole–Cole semicircles, implying that five dielectric relaxation processes are generated during the absorption of microwaves, which makes a significant contribution to the enhancement of its electromagnetic wave absorption performance.[40] Moreover, the frequency dependent Z_{in}/Z_0 values of the activated carbon@Fe_3O_4 composites with thickness of 5 mm were also calculated, as shown in Fig. 10. It can be observed that the Z_{in}/Z_0 value of the 74 wt% Fe_3O_4 sample is close to free space when the frequency is about 1.89 GHz, while that of the pure Fe_3O_4 NPs is nearly equal to 2.43 GHz. This indicates that the impedance matching properties of 74 wt% Fe_3O_4 are better in the low frequency band, and more microwaves will transmit into the absorber, which will result in better microwave absorption performance in the low frequency band.

The detailed microwave absorption performances of activated carbon@Fe_3O_4 composites and a comparison of other representative composites are summarized in Table 1.[18–20,41,42] As shown in Table 1, carbon materials are often composited with ferrites to optimize their microwave absorption properties. Thus, the composites simultaneously present both dielectric loss and magnetic loss, which are highly conducive to their microwave absorption performance. Moreover, this finding indicates that most of the composites based on carbon materials and ferrites have stronger microwave absorption ability in the frequency range of 2–18 GHz, in which above 90% microwave energy can be dissipated as the RL is below −10 dB. Moreover, the absorption frequency range of the as-prepared activated carbon@Fe_3O_4 composite in the present study is the lowest compared with those obtained in other investigations, and its absorption band shifts further to lower frequency as its thickness increases.

Overall, activated carbon@Fe_3O_4 composites with superior absorption performances in the low frequency band can be obtained by controlling the loading content of Fe_3O_4 NPs on activated carbon. Most importantly, the hydrothermal method used in our preparation is relatively simple with no need for complex reactions and treatments. Hence, the composite reported herein can be used as a promising electromagnetic wave absorbing material in the low frequency band of 0.5–3 GHz.

4. Conclusions

In summary, activated carbon@Fe_3O_4 composites were synthesized via the hydrothermal synthesis method, and their electromagnetic wave absorption performances were also investigated in the low frequency band of 0.5–3 GHz. Dielectric and magnetic loss both contribute to the electromagnetic wave absorption performance of the activated carbon@Fe_3O_4 composites, and the loading content of Fe_3O_4 NPs on activated carbon can modify their electromagnetic wave absorption properties. The maximum RL of −10.08 dB at 1.75 GHz with a −5 dB bandwidth over a broad frequency range of 1.55 GHz (1.07–2.62 GHz) was obtained when the percentage of Fe_3O_4 NPs and thickness of the composite were 74 wt% and 5 mm, respectively. This investigation presents a facile method to fabricate electromagnetic wave absorption composites with good performances in the low frequency band and suggests that activated carbon@Fe_3O_4 composites are promising candidates for electromagnetic wave absorption in the low frequency band of 0.5–3 GHz.

Conflicts of interest

There are no conflicts to declare.

Acknowledgements

References

1 X. Chen, F. Meng, Z. Zhou, X. Tian, L. Shan, S. Zhu, X. Xu, M. Jiang, L. Wang, D. Hui, Y. Wang, J. Lu and J. Gou, *Nanoscale*, 2014, **6**, 8140.

2 J. Ling, W. Zhai, W. Feng, B. Shen, J. Zhang and W. Zheng, *ACS Appl. Mater. Interfaces*, 2013, **5**, 2677.

3 A. K. Dhami, *Environ. Monit. Assess.*, 2012, **184**, 6507.

4 L. Kong, X. Yin, X. Yuan, Y. Yuan, Y. Zhang, X. Liu, L. Cheng and L. Zhang, *Carbon*, 2014, **73**, 185.

5 M. Han, D. Liang and L. Deng, *Appl. Phys. Lett.*, 2011, **99**, 082503.

6 H. Wang, Y. Dai, W. Gong, D. Geng, S. Ma, D. Li, W. Liu and Z. Zhang, *Appl. Phys. Lett.*, 2013, **102**, 223113.

7 H. Luo, W. Chen, W. Zhou, L. Long, L. Deng, P. Xiao and Y. Li, *Ceram. Int.*, 2017, **43**, 12328.

8 S. Yun, A. Kirakosyan, S. Surabhi, J. R. Jeong and J. Choi, *J. Mater. Chem. C*, 2017, **5**, 8436.

9 Y. Xu, L. Yuan, Z. Liang, X. Wang and X. Li, *J. Alloys Compd.*, 2017, **704**, 593.

10 O. Khani, M. Z. Shoushtari, K. Ackland and P. Stamenov, *J. Magn. Magn. Mater.*, 2017, **428**, 28.

11 D. L. Zhao and Z. M. Shen, *Mater. Lett.*, 2008, **62**, 3704.

12 N. Tang, Y. Yang, K. Lin, W. Zhong, C. Au and Y. Du, *J. Phys. Chem. C*, 2008, **112**, 10061.

13 R. H. Baughman, A. A. Zakhidov and W. A. de Heer, *Science*, 2002, **297**, 787.

14 L. Zhang, Q. Q. Ni, T. Natsuki and Y. Fu, *Appl. Surf. Sci.*, 2009, **255**, 8676.

15 Y. Shan, K. Chen, X. Yu and L. Gao, *Appl. Surf. Sci.*, 2010, **257**, 362.

16 X. L. Shi, M. S. Cao, J. Yuan and X. Y. Fang, *Appl. Phys. Lett.*, 2009, **95**, 163108.

17 F. S. Wen, F. Zhang and Z. Y. Liu, *J. Phys. Chem. C*, 2011, **115**, 14025.

18 B. Heidari, M. Ansari, A. Hoseinabadi, H. Jiriaee and F. Heidary, *J. Mater. Sci.: Mater. Electron.*, 2017, **28**, 1028.

19 Y. Wang, H. Y. Zhu, Y. B. Chen, X. M. Wu, W. Z. Zhang, C. Y. Luo and J. H. Li, *Mater. Chem. Phys.*, 2017, **202**, 184.

20 C. L. Hou, T. H. Li, T. K. Zhao, H. G. Liu, L. H. Liu and W. J. Zhang, *New Carbon Mater.*, 2013, **28**, 184.

21 P. Sardarian, H. N. Moosavy and S. S. S. Afghahi, *J. Magn. Magn. Mater.*, 2017, **441**, 257.

22 Y. Y. Lan, X. H. Li, Y. Zong, Z. X. Li, Y. Sun, G. G. Tan, J. Feng, Z. Y. Ren and X. L. Zheng, *Ceram. Int.*, 2016, **42**, 19110.

23 H. Deng, X. L. Li, Q. Peng, X. Wang, J. P. Chen and Y. D. Li, *Angew. Chem., Int. Ed.*, 2005, **117**, 2842.

24 A. M. Nicolson and G. F. Ross, *IEEE Trans. Instrum. Meas.*, 1970, **19**, 377.

25 X. Weng, B. Li, Y. Zhang, X. Lv and G. Gu, *J. Alloys Compd.*, 2017, **695**, 508.

26 J. P. Wang, J. Wang, R. X. Xu, Y. Sun, B. Zhang, W. Chen, T. Wang and S. Yang, *J. Alloys Compd.*, 2015, **653**, 14.

27 Y. M. Huang, Q. Qi, H. Pan, X. F. Lei and X. B. Liu, *J. Mater. Sci.: Mater. Electron.*, 2016, **27**, 9577.

28 D. Micheli, C. Apollo, R. Pastore and M. Marchetti, *Compos. Sci. Technol.*, 2010, **70**, 400.

29 X. F. Liu, X. R. Cui, Y. X. Chen, X. J. Zhang, R. H. Yu, G. S. Wang and H. Ma, *Carbon*, 2015, **95**, 870.

30 W. L. Song, M. S. Cao, M. M. Lu, J. Liu, J. Yuan and L. Z. Fan, *J. Mater. Chem. C*, 2013, **1**, 1846.

31 X. F. Zhang, X. L. Dong, H. Huang, Y. Y. Liu, W. N. Wang, X. G. Zhu, B. Lv and J. P. Lei, *Appl. Phys. Lett.*, 2006, **89**, 053115.

32 K. Butter, P. H. H. Bomans, P. M. Frederik, G. J. Vroege and A. P. Philipse, *Nat. Mater.*, 2003, **2**, 88.

33 H. Zhao, X. Sun, C. Mao and J. Du, *Phys. B*, 2009, **404**, 69.

34 S. S. Kim, S. T. Kim, Y. C. Yoon and K. S. Lee, *J. Appl. Phys.*, 2005, **97**, 10F905.

35 B. S. Zhang, Y. Feng, J. Xiong, Y. Yang and H. X. Lu, *IEEE Trans. Magn.*, 2006, **42**, 1778.

36 L. Qiao, R. Han, T. Wang, L. Y. Tang and F. S. Li, *J. Magn. Magn. Mater.*, 2015, **375**, 100.

37 R. Li, T. Wang, G. G. Tan, W. L. Zuo, J. Q. Wei, L. Qiao and F. S. Li, *J. Alloys Compd.*, 2014, **586**, 239.

38 I. W. Nam, H. K. Lee and J. H. Jang, *Composites, Part A*, 2011, **42**, 1110.

39 Y. C. Du, W. W. Liu, R. Qiang, Y. Wang, X. J. Han, J. Ma and P. Xu, *ACS Appl. Mater. Interfaces*, 2014, **6**, 12997.

40 L. Y. Zhu, X. J. Zeng, M. Chen and R. H. Yu, *RSC Adv.*, 2017, **7**, 26801.

41 L. N. Wang, X. L. Jia, Y. F. Li, F. Yang, L. Q. Zhang, L. P. Liu, X. Ren and H. T. Yang, *J. Mater. Chem. A*, 2014, **2**, 14940.

42 M. S. Cao, J. Yang, W. L. Song, D. Q. Zhang, B. Wen, H. B. Jin, Z. L. Hou and J. Yuan, *ACS Appl. Mater. Interfaces*, 2012, **4**, 6949.